

CrossMark  
click for updatesCite this: *J. Mater. Chem. A*, 2017, 5, 4047

## Sandwich-structured cathodes with cross-stacked carbon nanotube films as conductive layers for high-performance lithium-ion batteries†

Lingjia Yan, Ke Wang, Shu Luo, Hengcai Wu, Yufeng Luo, Yang Yu, Kaili Jiang, Qunqing Li, Shoushan Fan and Jiaping Wang\*

A simple and feasible strategy of using cross-stacked super-aligned carbon nanotube (SACNT) films as conductive layers to prepare sandwich-structured LiCoO<sub>2</sub> cathodes for high-performance lithium-ion batteries (LIBs) is reported. Owing to the super-aligned feature, the SACNTs are fully dispersed and form a homogeneous and efficient conductive network in the electrodes. Meanwhile, the sandwiched electrode structure, consisting of a repeating and alternating stack of LiCoO<sub>2</sub> layers and SACNT films, ensures that each layer of active materials can adhere to the SACNT conductive layers, realizing sufficient electron transfer throughout the electrodes regardless of the thickness of the electrodes. With the introduction of three separate SACNT conductive layers, significant improvements on the conductivity as well as the cell performance are achieved. The sandwich-structured LiCoO<sub>2</sub>-2 wt% Super P-SACNT cathodes possess an impressive rate capability (109.6 mA h g<sup>-1</sup> at 10C and 1668% improvement compared with that without SACNT films), showing the best rate performances reported so far for commercial micro-sized LiCoO<sub>2</sub> particles. The easy fabrication procedure, compatible method for commercialization, low cost, and outstanding electrochemical performances of the sandwich-structured electrode demonstrate its great potential for the large-scale production of high-performance electrodes for LIBs.

Received 20th November 2016  
Accepted 12th January 2017

DOI: 10.1039/c6ta10024d

www.rsc.org/MaterialsA

### Introduction

Rechargeable lithium-ion batteries (LIBs) are widely used in electronic devices such as mobile phones, digital cameras or laptops, as well as in electric vehicles owing to their high energy density, long cycle lifetime, excellent rate performance, and environmentally friendly nature.<sup>1-4</sup> Of the traditional commercial LIBs, LiCoO<sub>2</sub>, LiMn<sub>2</sub>O<sub>4</sub>, and LiFePO<sub>4</sub> are the most widely used candidates for cathode active materials. However, all of these candidates share the common problem of poor electrical conductivity. The conductivities of LiCoO<sub>2</sub>, LiMn<sub>2</sub>O<sub>4</sub>, and LiFePO<sub>4</sub> are as low as 10<sup>-3</sup> S cm<sup>-1</sup>, 10<sup>-4</sup> S cm<sup>-1</sup>, and 10<sup>-9</sup> S cm<sup>-1</sup>, respectively, leading to the incomplete use of the active materials and severe polarization.<sup>5-8</sup> Many methods, including the modification of the active material by lattice doping, surface coating, and the addition of various conducting agents<sup>9-15</sup> have been exploited to solve this problem. Among them, the addition of conductive additives is the most widely used strategy in the industrial production of LIBs, due to their relatively low cost and compatibility with large-scale production. However, the

commonly used conducting agents usually possess poor crystallinity (Super P) or a small specific area (graphite), and their efficiency to form a continuous and highly conductive network throughout the electrode composite is limited. As a result, the proportion of these electrochemically inactive conducting agents are often as high as 10 wt% for general testing and even 20 wt% for high rate testing seriously reducing the energy densities of the electrodes. To decrease the amount of conductive additives, various kinds of carbon nanomaterials such as carbon nanofibers,<sup>16,17</sup> carbon nanotubes,<sup>18-22</sup> and graphenes,<sup>23-25</sup> have been used taking advantage of their higher aspect ratio and superiority in forming long-range conducting pathways. Previous results have shown that improved performance, such as better cycling stability and higher rate capacity, can be achieved with this strategy.<sup>26,27</sup> Nevertheless, great difficulties are encountered when dispersing these nano-sized carbon agents by the common mechanical process. Consequently, extra treatments, including chemical oxidation,<sup>28</sup> ultrasonication,<sup>29,30</sup> and surface coating<sup>12</sup> are usually required to solve the aggregation problem. In fact, extensive studies based on these strategies have been reported with impressive cell performances at the laboratory scale. Unfortunately, for industrial production, these sophisticated routes will become much less feasible because of the limitation of the cost and the complex fabrication procedures. Another distinction between the laboratory samples and

Department of Physics and Tsinghua-Foxconn Nanotechnology Research Center, Tsinghua University, Beijing 100084, China. E-mail: jpwang@tsinghua.edu.cn

† Electronic supplementary information (ESI) available. See DOI: 10.1039/c6ta10024d

commercial products is the thickness of the electrode. For laboratory samples, it is possible to improve the cell performance by reducing the thickness, as a thinner electrode usually means a smaller distance for charge transportation. Actually, the excellent rate performances reported in the literature have generally been based on thin electrodes with thicknesses below 40  $\mu\text{m}$ .<sup>30–32</sup> Besides, it is worth noting that the specific capacity decreases as the thickness of the electrode increases.<sup>32</sup> However, it is difficult for such thin electrodes to meet the demand of high energy densities (based on the total mass of the cathode including current collectors) of commercial LIBs as a result of the limited active material loading. Therefore, the development of a facile strategy is essential, which can not only achieve enhanced battery performances but can also meet the industrial requirements.

Herein, a simple but efficient strategy is proposed to improve the cell performance of a conventional  $\text{LiCoO}_2$ -Super P electrode by introducing cross-stacked super-aligned CNT (SACNT) films as the conductive layers. Owing to the super-aligned feature, the agglomeration of SACNTs could easily be avoided by just drawing continuous films from the SACNT arrays,<sup>33–37</sup> and a highly efficient conductive layer could be fabricated by simply cross-stacking the SACNT films on the surface of the  $\text{LiCoO}_2$  electrodes. Even though the addition of SACNT films is quite simple and fast, these carbon additives are highly dispersed,

and a negligible amount of SACNTs have led to a notable improvement on the charge transportation. In fact, only two layers of the SACNT films, which account for less than 0.04 wt% of the total mass of the electrode, have increased the electrical conductivity of the  $\text{LiCoO}_2$ -2 wt% Super electrode by one order of magnitude, and excellent cycling stability was realized. In addition, a novel sandwich-electrode structure was obtained by simply repeating the procedure of casting the  $\text{LiCoO}_2$  slurry and stacking the SACNT film alternatively several times, as schematically shown in Fig. 1. The layer-by-layer electrode construction ensured that nearly all the  $\text{LiCoO}_2$  particles were able to adhere to the SACNT conductive layers directly, leading to sufficient electron transfer as well as efficient inhibition of polarization, regardless of the total thickness of the electrode. Thus, there was no need to reduce the thickness of the electrode and the active material loading to obtain decent rate performance. The sandwich-structured  $\text{LiCoO}_2$ -2 wt% Super P-SACNT cathode, with a thickness compatible with commercial LIBs, delivered a specific discharge capacity of 109.6  $\text{mA h g}^{-1}$  at 10C, which is one of the best values reported so far for commercial micro-sized  $\text{LiCoO}_2$  powders.<sup>38–41</sup> Meanwhile, much higher energy densities (based on whole electrodes) were realized in the sandwich-structured electrodes, which were ascribed to the increase in electrical conductivity together with the reduction of the carbon additives. Moreover, this electrode fabrication process

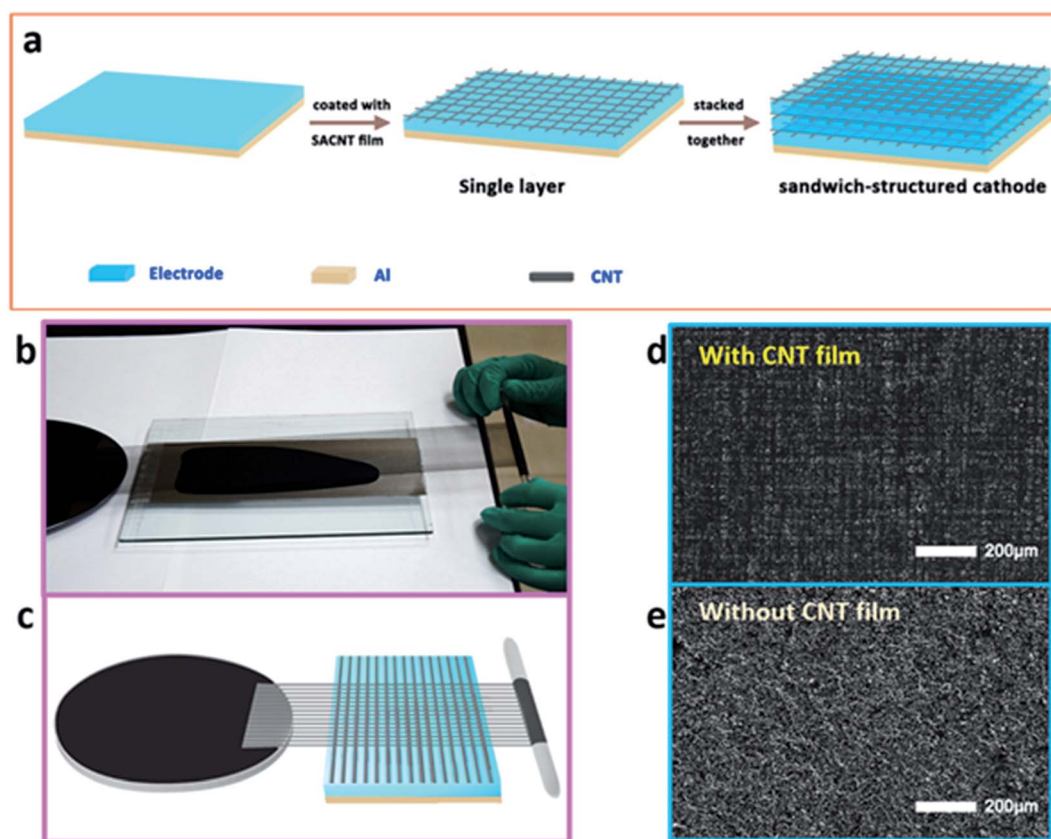


Fig. 1 (a) Schematic of the fabrication procedure for a sandwich-structured cathode containing multiple  $\text{LiCoO}_2$ -Super P layers, coated with a cross-stacked SACNT film as the conductive layer. (b and c) Photograph and schematic of the coating of a cross-stacked SACNT film. Top surface SEM images of the three-layer  $\text{LiCoO}_2$ -2 wt% Super P electrodes: (d) with and (e) without the SACNT film.

can be easily scaled up, and it will have great potential to improve the electrochemical performance of the commercial batteries.

## Experimental section

### Material preparation

LiCoO<sub>2</sub> powders (Reshine, China), carbon black powders (50 nm in diameter, Timcal Ltd., Switzerland), *N*-methyl-2-pyrrolidinone (NMP), and polyvinylidene difluoride (PVDF) were used as the active material, conducting agent, dispersant, and binder, respectively. LiCoO<sub>2</sub> and PVDF were mixed together at a weight ratio of 8 : 1, and the amount of Super P was 2 wt% or 5 wt%. The cathode material, conducting agent, as well as the PVDF binder were dispersed in NMP and ground in a mortar for approximately 20 min. The resulting slurry was uniformly spread on aluminum foil (20 μm in thickness) (Fig. 1a). SACNT arrays with a height of 300 μm and a diameter of 20–30 nm were synthesized on 4-inch silicon wafers in a low-pressure chemical vapor deposition (LP-CVD) system with iron as the catalyst and acetylene as the precursor. The preparation details can be found elsewhere.<sup>33,35,42</sup> SACNT films were drawn from the SACNT arrays, following an end-to-end joining mechanism.<sup>35</sup> The SACNT films were cross-stacked onto the LiCoO<sub>2</sub> electrode to form one conductive layer (Fig. 1b and c). The single-layer LiCoO<sub>2</sub>-Super P-SACNT cathodes were fabricated by applying this process once, while the sandwich-structured cathodes were made by repeating the procedure of casting the LiCoO<sub>2</sub> slurry and cross-stacking the SACNT films alternatively three times (Fig. 1a). The conventional LiCoO<sub>2</sub>-Super P cathodes were fabricated by the same process but without applying the SACNT films, and their thickness was controlled to be close to that of the corresponding LiCoO<sub>2</sub>-Super P-SACNT electrodes. Besides, a randomly oriented carbon nanotube (RCNT, 5–20 nm in diameter and 1–10 μm in length, Chengdu Organic Chemicals Ltd., China) was used as the conducting agent to prepare the control sample. The LiCoO<sub>2</sub>-10 wt% RCNT cathode was fabricated by the same procedures as for the LiCoO<sub>2</sub>-Super P electrode. After drying at 70 °C for approximately 30 min, the electrode sheets were punched into circular discs with a diameter of 10 mm. Before the cell assembly, all the electrodes were dried again in a vacuum oven for 24 h at 120 °C, to evaporate the dispersant completely.

### Material analysis

The microstructure and morphology of the LiCoO<sub>2</sub> electrodes were examined with an FEI Sirion 200 scanning electron microscope (SEM) operating at 10 kV. The particle size distribution of the LiCoO<sub>2</sub> powders was studied using a Mastersizer 2000 laser particle characterization system (Malvern Instruments Ltd., UK). The crystalline structures of LiCoO<sub>2</sub> powders were characterized by X-ray diffraction (XRD) using a diffractometer (Rigaku, Cu K $\alpha$  radiation). The diffraction patterns were collected in the 2 $\theta$  range from 10° to 80°. The conductivities of the LiCoO<sub>2</sub> electrodes were measured by a four-point probe method.

### Electrochemical measurements

All electrochemical characterizations were performed using CR2016 coin-type cells. The cell assembly was carried out in an Ar-filled glove box (M. Braun Inert Gas Systems Co. Ltd.) with both moisture and oxygen levels below 0.1 ppm. LiCoO<sub>2</sub>-Super P cathodes with and without the SACNT conductive layers were used as the working electrodes, and lithium foils were used as the counter electrodes for all measurements. A porous polymer film (Celgard 2400, USA) was used to separate the cathode and the anode. The electrolyte was a 1.0 M LiPF<sub>6</sub> solution in ethylene carbonate (EC) and diethyl carbonate (DEC) mixed at a volume ratio of 1 : 1. The galvanostatic charge-discharge process was conducted with a battery testing system (Wuhan Land Electronic Co., China) from 3.0 to 4.3 V. Cyclic voltammetry tests were conducted using a potentiostat/galvanostat (EG&G Princeton Applied Research 273A) at a scan rate of 0.1 mV s<sup>-1</sup> in the range of 3.0–4.3 V. Electrochemical impedance spectroscopy (EIS) was performed on the same electrochemical system with a small perturbation voltage of 5 mV while the frequency range was from 100 mHz to 100 kHz. All the electrochemical tests were performed at room temperature and in an ambient atmosphere.

## Results and discussion

As illustrated in Fig. 1a–c, the fabrication procedure of the sandwich-structured LiCoO<sub>2</sub>-Super P-SACNT electrodes was quite convenient and compatible with that of conventional LIBs, with only the additional step of stacking the SACNT films. The crystalline structure of the LiCoO<sub>2</sub> powders is displayed in Fig. S1.† SEM images of the top surfaces of the LiCoO<sub>2</sub>-Super P-SACNT electrode and the LiCoO<sub>2</sub>-Super P electrode are shown in Fig. 1d and e. On the LiCoO<sub>2</sub>-Super P-SACNT composite, the SACNT films were spread in two perpendicular directions, forming a uniform and long-range conductive network across the surface of the electrode; while for the LiCoO<sub>2</sub>-Super P cathode, there was no such conductive pathway (Fig. 1e), and the connections between the active materials were merely constructed by the small and separate Super P powders. This distinct difference on the surface morphology would have a great influence on the conductivity as well as the cell performance. Yet, before making an overall comparison, it was reasonable to determine the optimal parameters of the LiCoO<sub>2</sub>-Super P-SACNT electrode. Considering that the sandwich-structured cathode consisted of repeated structural units, a single-layer LiCoO<sub>2</sub>-Super P cathode was chosen as the starting point to optimize the amount of Super P and the layers of cross-stacked SACNT films in one conductive layer.

SEM images of the cross-section and the top surface of the single-layer LiCoO<sub>2</sub>-Super P cathode covered with a 2-layer cross-stacked SACNT film are shown in Fig. 2a and b. It can be seen that the cathode has a thickness of approximately 25 μm, with the cross-stacked SACNT films adhering to the top surface. Besides, the magnified image in Fig. 2b shows that the SACNTs were highly dispersed, indicating the full use of the CNTs to improve the electron transport capability of the electrodes. A similar morphology was also observed on the LiCoO<sub>2</sub>-Super P

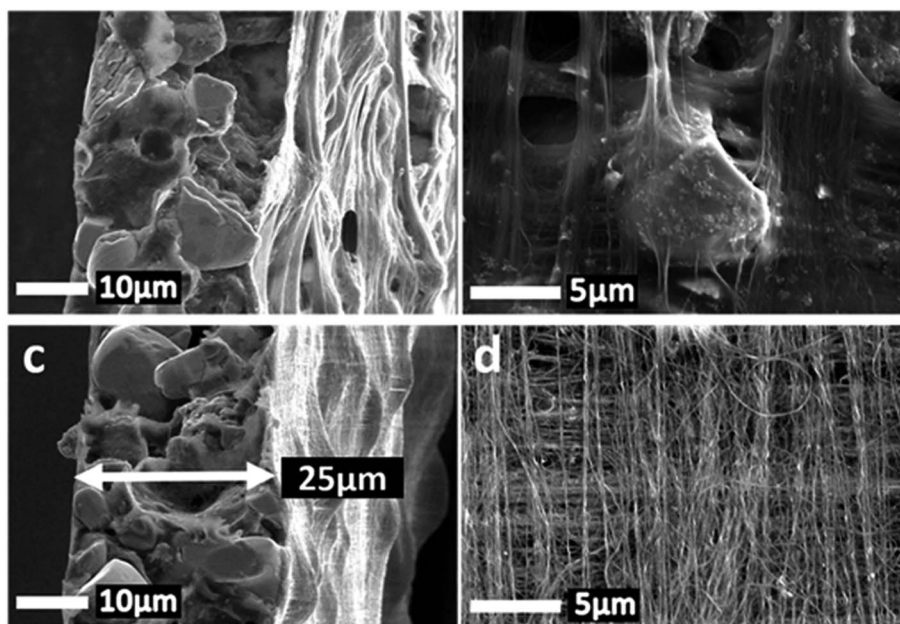


Fig. 2 Cross-sectional SEM images of the single-layer  $\text{LiCoO}_2$ -2 wt% Super P cathodes covered with a (a) 2-layer and (c) 10-layer cross-stacked SACNT film. (b) and (d) are the top surface morphologies of (a) and (c), respectively.

electrode covered with a 10-layer cross-stacked SACNT film, as shown in Fig. 2c and d. The only difference lies in the slightly increased thickness and denser CNT coverage on the surface of the  $\text{LiCoO}_2$  electrode. Despite all this, the thickness of the SACNT films was almost negligible in comparison with that of the electrodes for both kinds of conductive layers. Moreover, considering that the areal density of a single layer of SACNT film was  $2 \times 10^{-3} \text{ mg cm}^{-2}$ , these conductive layers only accounted for a small fraction of the overall weight of the electrode. In particular, the proportion of the 2-layer SACNT film was less than 0.04 wt%, which could be regarded as a negligible contribution to the mass fraction of the conductive agent.

To optimize the amount of Super P in the cathodes, the electrical conductivities of the single-layer  $\text{LiCoO}_2$  electrodes containing 2 wt% and 5 wt% Super P with various layers of

SACNT films are compared in Fig. 3a. The electrical conductivity of the  $\text{LiCoO}_2$ -2 wt% Super P cathode was only  $1.0 \times 10^{-3} \text{ S cm}^{-1}$ . By introducing a 2-layer cross-stacked SACNT film as the conductive layer, the conductivity was boosted by an order of magnitude and reached  $3.1 \times 10^{-2} \text{ S cm}^{-1}$ . As the number of SACNT layers was further increased to 4 and 10, the conductivities gradually increased to  $6.1 \times 10^{-2} \text{ S cm}^{-1}$  and  $1.6 \times 10^{-1} \text{ S cm}^{-1}$ , respectively. Such a significant influence on the conductivity of the  $\text{LiCoO}_2$ -2 wt% Super P cathode by introducing SACNT films can be attributed to their high conductivity and large aspect ratio. Generally, a SACNT film displayed a conductivity of  $3.0 \times 10^2 \text{ S cm}^{-1}$ .<sup>43</sup> In contrast, Super P as a spherical carbon black powder, possessed a conductivity of only  $1.4 \times 10^{-1} \text{ S cm}^{-1}$ .<sup>44</sup> The conductivity of the  $\text{LiCoO}_2$ -5 wt% Super P cathode was  $4.8 \times 10^{-2} \text{ S cm}^{-1}$ , which was higher than

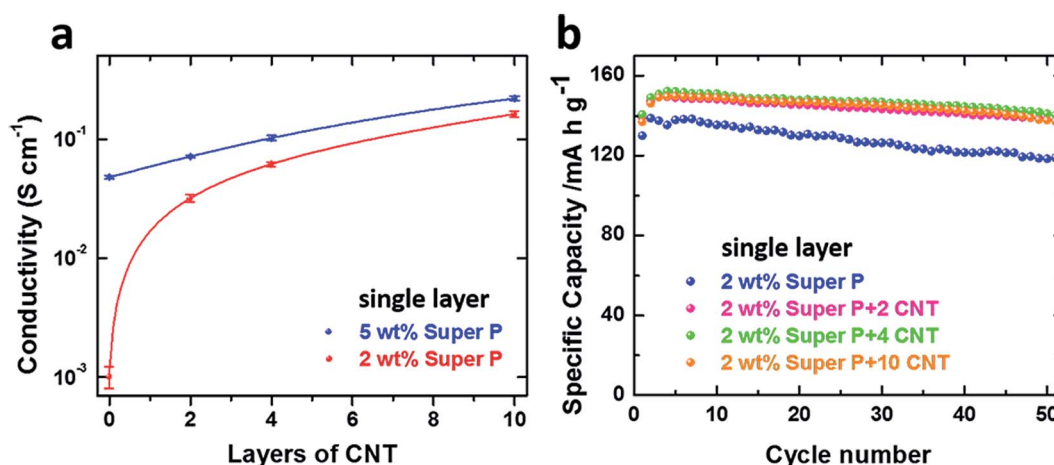


Fig. 3 (a) Electrical conductivities of single-layer  $\text{LiCoO}_2$  cathodes containing 2 wt% and 5 wt% Super P, and (b) cycling performance of single-layer  $\text{LiCoO}_2$ -2 wt% Super P cathodes at 0.1C covered with various layers of the cross-stacked SACNT film.

that of the LiCoO<sub>2</sub>-2 wt% Super P cathode. As the number of layers of the cross-stacked SACNT film was increased from 2 to 4 and 10, the LiCoO<sub>2</sub>-5 wt% cathodes demonstrated a gradual and slower increase in the electrical conductivity, compared with that of the LiCoO<sub>2</sub>-2 wt% Super P-SACNT cathodes. Besides, the electrical conductivities of the LiCoO<sub>2</sub>-2 wt% Super P cathodes with a SACNT conductive layer were close to those of the corresponding cathodes with 5 wt% Super P. Considering the demand to reduce the amount of inert materials, 2 wt% was chosen as the optimized proportion of Super P.

The influence of the number of SACNT films in one conductive layer was detected by the galvanostatic charge-discharge measurement. The cycling performance of the single-layer LiCoO<sub>2</sub>-2 wt% Super P cathode and the LiCoO<sub>2</sub>-2 wt% Super P-SACNT cathodes with 2, 4, and 10 CNT layers were examined at 0.1C (Fig. 3b). The initial specific capacity of the single-layer LiCoO<sub>2</sub>-Super P cathode was 136 mA h g<sup>-1</sup>, with a capacity retention of 85.3% after 50 cycles. However, for the cathode with a 2-layer cross-stacked SACNT film, the initial specific capacity was 149 mA h g<sup>-1</sup> and the capacity retention was higher than 92% over 50 cycles. As the number of layers of CNT films was increased to 4 or 10, the electrodes demonstrated almost identical performance with the cathode with a 2-layer SACNT film, which was consistent with the electrical conductivity results. Consequently, a conductive layer composed of

a 2-layer cross-stacked SACNT film was sufficient to improve the cell performance, while the proportion of the conducting agent in the LiCoO<sub>2</sub>-2 wt% Super P-SACNT electrode could be treated as being the same as that of the LiCoO<sub>2</sub>-2 wt% Super P electrodes.

Based on the optimized parameter achieved above, the sandwich-structured LiCoO<sub>2</sub>-2 wt% Super P-SACNT cathodes were fabricated, where each structural unit consisted of a 2-layer cross-stacked SACNT film as the conductive layer. Fig. 4a displays the cross-sectional SEM image of the LiCoO<sub>2</sub>-Super P-SACNT electrode. In this electrode, the LiCoO<sub>2</sub> layers were sandwiched between three SACNT layers, which served as continuous conductive layers along the lateral direction. For comparison, the cross-sectional SEM image of the LiCoO<sub>2</sub>-Super P cathodes without the SACNT film is illustrated in Fig. 4b, from which only bare LiCoO<sub>2</sub>, Super P, and PVDF particles were observed, and no continuous conductive component across the electrode existed. Such a difference in the electrode morphology indicates that the LiCoO<sub>2</sub>-Super P-SACNT cathodes are more competitive with regard to the long-range electron transportation capability. This viewpoint was confirmed by the comparison of the conductivity of these two types of electrodes with almost the same thickness. The conductivity of the sandwich-structured LiCoO<sub>2</sub>-Super P-SACNT electrode was as high as  $5.5 \times 10^{-2}$  S cm<sup>-1</sup>, compared with only  $2.4 \times 10^{-3}$  S cm<sup>-1</sup> for the LiCoO<sub>2</sub>-Super P electrode.

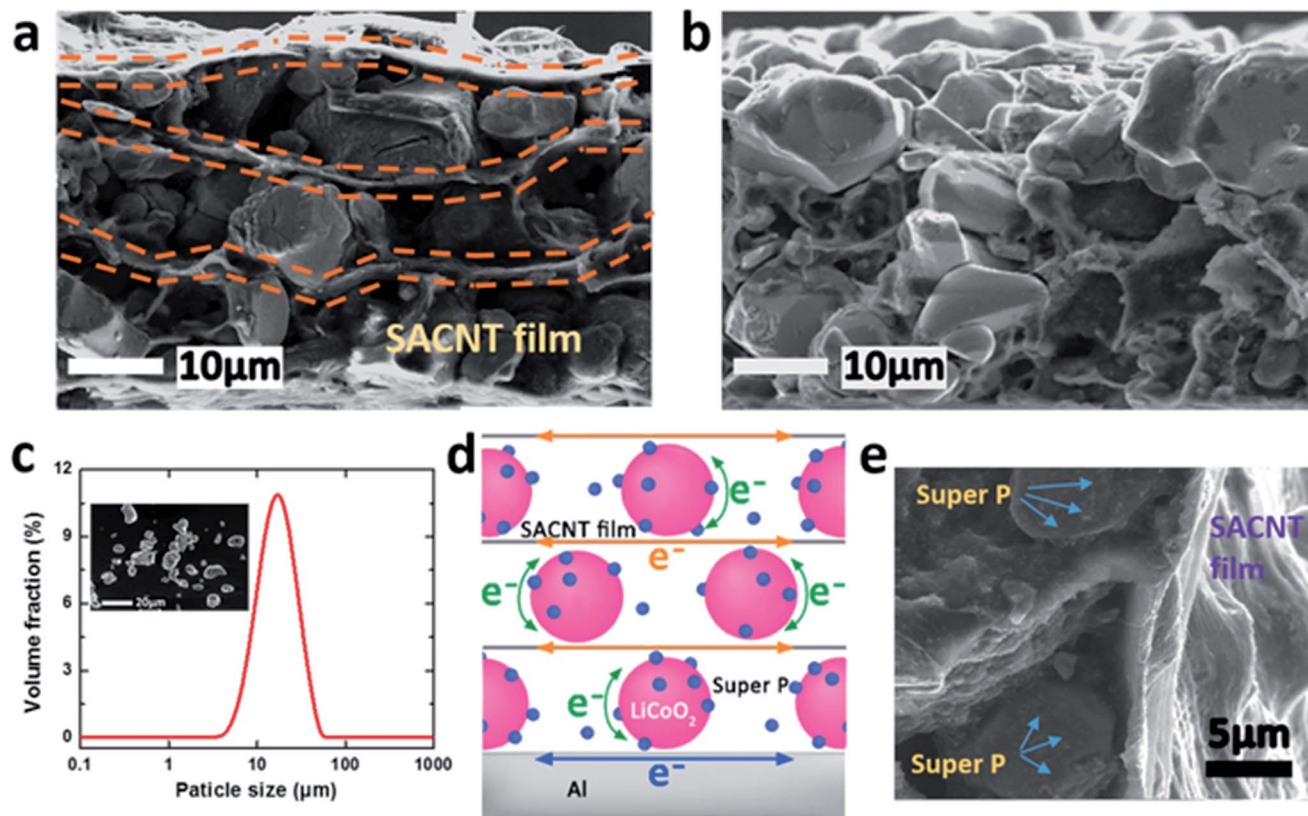


Fig. 4 Cross-sectional SEM image of the three-layer LiCoO<sub>2</sub>-Super P cathodes (a) with and (b) without the SACNT film. (c) Size distribution of LiCoO<sub>2</sub> particles. The inset photograph shows the SEM image of LiCoO<sub>2</sub> particles. (d) Schematic of the cross-sectional structure of the sandwich-structured LiCoO<sub>2</sub>-Super P-SACNT electrode, demonstrating the electron transfer pathways by both Super P powders and the SACNT film. (e) SEM image of a LiCoO<sub>2</sub> electrode with both the conductive layer and the conductive agent.

To gain a greater understanding of the roles of the SACNT conductive layers and the sandwich structure in affecting the performances of the LiCoO<sub>2</sub> electrode, the inner structure and electron transfer process in the electrodes were deeply investigated. Fig. 4c reveals that the average size of the LiCoO<sub>2</sub> particle was approximately 15–20 μm. Coincidentally, the distance between each conductive CNT layer in the LiCoO<sub>2</sub>-Super P-SACNT electrode was also approximately 15–20 μm, as shown in Fig. 4a. Consequently, the sandwich-structured electrode could be regarded as a repeating and alternating stack of the SACNT films and a LiCoO<sub>2</sub> particle layer, which is schematically illustrated in Fig. 4d. This layer-by-layer electrode structure ensured that almost all the LiCoO<sub>2</sub> particles were able to connect with the adjacent SACNT layers directly. The long-range electron transport paths (orange arrows) across the separate LiCoO<sub>2</sub> particles, especially along the lateral direction, could be sufficiently fulfilled by the SACNT conductive layers. In comparison, the conventional conductive agent Super P displayed much lower efficiency for long-range electron transport. As shown in the magnified SEM images in Fig. 4e, the spherical Super P powders tended to form short-range conductive networks. Thus, in the LiCoO<sub>2</sub>-Super P electrodes, only the LiCoO<sub>2</sub> particles adjacent to the Al foil could realize sufficient long-range electron transportation with the benefit of the current collector. For the active materials further away from the Al foil, polarization may be inevitable owing to the lack of long-range electron transport paths. As the electrode thickness increased, more serious polarization occurred, which was one of the main reasons for the poor rate capability of thick electrodes. In the LiCoO<sub>2</sub>-Super P-SACNT electrode, both long-range and short-range electron transport pathways could be well satisfied by SACNT conductive layers (orange arrow in Fig. 4d) and Super P powders (green arrow in Fig. 4d), respectively, regardless of the thickness of the electrode. Such homogeneous and hybrid conductive networks could prevent uneven electron distribution, and increase the use of active materials in the electrochemical reactions. As a result, better cell performance could be expected for the sandwich-structure electrodes.

The electrochemical performance of the LiCoO<sub>2</sub>-Super P cathodes with and without the SACNT conductive layer was first evaluated by comparing the galvanostatic charge/discharge curves of the 1<sup>st</sup> cycle at 0.1C. As shown in Fig. 5a, the sandwich-structured LiCoO<sub>2</sub>-Super P-SACNT electrode displayed a much 'flatter' voltage profile, while the LiCoO<sub>2</sub>-Super P electrode presented a larger potential difference between the charge and discharge plateaus. The difference in the charge/discharge curves reflected a lower degree of polarization in the sandwich-structured electrode, indicating a better electron transfer capability. This opinion could also be confirmed by the specific capacity, since polarization usually acts as a hindrance to making full use of the active materials. In the first cycle, the LiCoO<sub>2</sub>-Super P-SACNT electrode exhibited a specific discharge capacity of 153.6 mA h g<sup>-1</sup>, whereas the LiCoO<sub>2</sub>-Super P electrode had a capacity of only 139.0 mA h g<sup>-1</sup>.

Fig. 5b shows the cyclic voltammetry profiles of LiCoO<sub>2</sub>-Super P and LiCoO<sub>2</sub>-Super P-SACNT cathodes in the second

cycle. Generally speaking, the shapes of the redox peaks in a CV curve can reflect the charge-discharge reaction kinetics of Li<sup>+</sup> insertion/deinsertion. The peak profiles of the sandwich-structured electrode were sharper than that of LiCoO<sub>2</sub>-Super P, indicating faster Li<sup>+</sup> insertion/deinsertion and smaller conductivity restrictions. The superiority in the reaction kinetics also stemmed from the SACNT conductive layers in the sandwich-structured LiCoO<sub>2</sub>-Super P-SACNT electrodes. The cross-stacked SACNT films could not only supply efficient pathways for electron transfer, but also improve the transportation of Li<sup>+</sup> ions, as the large number of micropores in the CNT films was very beneficial for the penetration of the electrolyte into the composites.

Cycling performances of the LiCoO<sub>2</sub>-Super P and LiCoO<sub>2</sub>-Super P-SACNT cathodes were examined at 0.1C (Fig. 5c). The initial specific capacity of the LiCoO<sub>2</sub>-Super P cathode was 135.2 mA h g<sup>-1</sup>, and faded to 126.7 mA h g<sup>-1</sup> after 50 cycles. Since the content of Super P was only 2 wt% and the nanometer-sized Super P powders tended to aggregate, it was difficult for the Super P powders to distribute homogeneously and form a continuous conductive network in the LiCoO<sub>2</sub> electrode. Thus, serious electrode polarization was inevitable, and charge accumulation became severe along with the repeated reactions, leading to the apparent capacity loss. However, the multilayered conductive networks formed by the SACNT films provided uniform pathways to transport electrons throughout the whole electrode, as previously mentioned, thus the charge accumulation could be effectively avoided. In accordance with expectations, the sandwich-structured LiCoO<sub>2</sub>-Super P-SACNT cathodes not only exhibited a higher initial specific capacity, but also possessed more stable cycle performance. After 50 cycles, the specific discharge capacity of the LiCoO<sub>2</sub>-Super P-SACNT cathode was still as high as 146.0 mA h g<sup>-1</sup>, indicating that the capacity retention was higher than 95%, with capacity fading as low as 0.098% per cycle.

The specific capacities of the two types of cathodes were also investigated at various discharge rates while being charged at a constant rate of 0.1C (Fig. 5d). The electrochemical reactions under high current established more rigorous criteria for charge transportation, and the rate test results further strengthened the superiority of the sandwich-structured electrode. At a rate of 5C, the LiCoO<sub>2</sub>-Super P-SACNT electrode delivered a specific discharge capacity of 128.3 mA h g<sup>-1</sup>, which was even better than that of the LiCoO<sub>2</sub>-Super P electrode at a rate of 1C (126.4 mA h g<sup>-1</sup>). Additionally, the rate performance gap was widened as the rate was increased to 10C. The specific capacity of the sandwich-structured LiCoO<sub>2</sub>-Super P-SACNT cathode still remained as high as 109.6 mA h g<sup>-1</sup>, whereas the LiCoO<sub>2</sub>-Super P cathode almost failed (6.2 mA h g<sup>-1</sup>). Actually, the LiCoO<sub>2</sub>-Super P-SACNT electrode demonstrated one of the best rate performances reported so far for commercial micro-sized LiCoO<sub>2</sub> powders. Moreover, this outstanding rate capability was not based on thin cathodes, but on the electrodes with thicknesses near to those used in commercial LIBs. These results show good agreement with the discussion about the electron transfer process mentioned above. In the sandwich-structured electrodes, the multi-conductive layers guaranteed

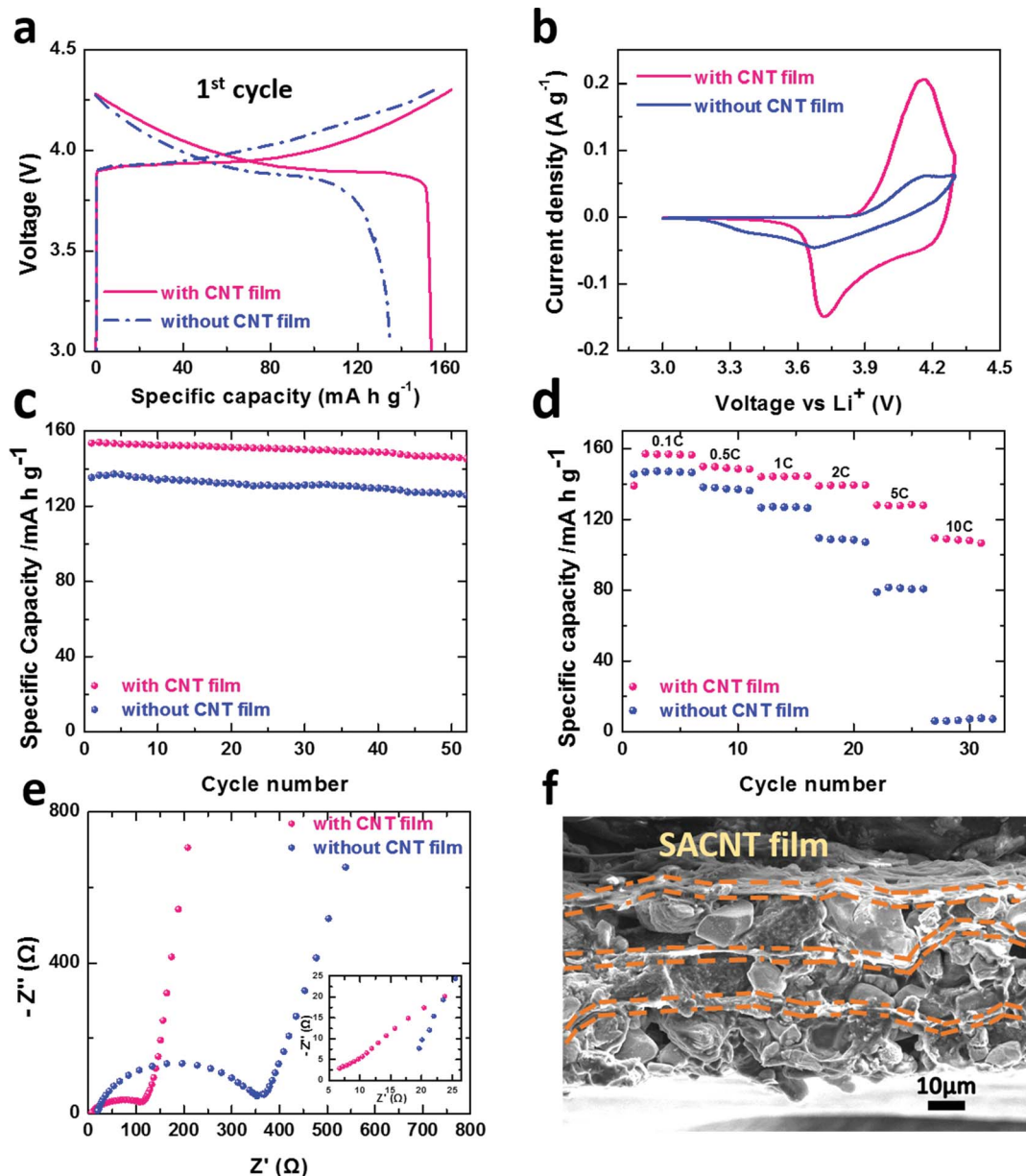


Fig. 5 (a) Charge/discharge curves in the 1<sup>st</sup> cycle, (b) CV curve at the 2<sup>nd</sup> cycle, (c) cycling (0.1C), (d) rate performance, and (e) the electrochemical impedance spectroscopy data of the three-layer LiCoO<sub>2</sub>-Super P cathodes with and without the SACNT film. The inset gives the enlarged view of the high-frequency part. (f) Cross-sectional SEM image of the three-layer LiCoO<sub>2</sub>-Super P-SACNT cathode after 50 cycles.

adequate electron transportation for the LiCoO<sub>2</sub> particles, no matter whether they were adjacent to the current collectors. Additionally, the porous cross-stacked SACNT films also provided extra routes for the penetration of the electrolytes, shortening the diffusion distance of Li<sup>+</sup> ions. Moreover, this advantage in the sandwich-structured cathodes would not be weakened by thickening the electrodes, since this kind of electrode could be regarded as a series of repeated elements composed of SACNT film-LiCoO<sub>2</sub> layers, and the increase in thickness arose from just adding another layer with the same construction. As thicker electrodes signify higher energy storage in a unit area, these sandwich-structured LiCoO<sub>2</sub>-Super

P-SACNT electrodes are competitive in meeting the requirement of practical application.

The effect of sandwich-structured SACNT conductive layers on the electrochemical characteristics was also studied by EIS. The common features of EIS spectra of the LiCoO<sub>2</sub>-Super P-SACNT and LiCoO<sub>2</sub>-Super P cathodes were that there was a depressed semicircle at the high-frequency region and a straight line at the low-frequency region (Fig. 5e). The cross points with the real axis at the high-frequency part are related to the ohmic resistance  $R_{\Omega}$  and the diameter of the semicircle represented the charge transfer resistance  $R_{ct}$ . The inset of Fig. 5e shows the enlarged view of the high-frequency range. In

fact,  $R_{\Omega}$  reflected the inner resistance including the resistance between the two electrodes, electrolyte, and separator. Considering the only difference between these two kinds of cells was the inner structure of the working electrodes, the smaller  $R_{\Omega}$  of the LiCoO<sub>2</sub>-Super P-SACNT electrodes (6.7  $\Omega$ ), in comparison with that of LiCoO<sub>2</sub>-Super P cathodes (19.6  $\Omega$ ), further proved that the addition of SACNT conductive layers significantly increased the electrical conductivity. In addition,  $R_{ct}$  values were 113.9  $\Omega$  and 353.5  $\Omega$  for the electrodes with and without SACNT conductive layers. The pronounced difference indicated that the charge transfer kinetic process can be improved by the sandwich-structured SACNT conductive layers, which corresponds to the improved performances of the LiCoO<sub>2</sub>-Super P-SACNT electrodes.

The microstructure of the LiCoO<sub>2</sub>-Super P-SACNT electrode after 50 cycles was further analyzed by SEM. There was no evident change of the sandwiched structure (Fig. 5f). Three SACNT conductive layers could be easily seen in the cross-sectional image. With the resilient SACNT films, the cathode presented a well-maintained microstructure similar to that before cycling. Although the cathode experienced long-time charging and discharging, the conductive SACNT layers with superior flexibility provided the cathode with adequate electron transportation during the whole cycle process. The SACNT conductive layers can effectively confine the LiCoO<sub>2</sub> particles

and sufficiently accommodate the volume expansion, resulting in a stable structure of the electrode. In consequence, the sandwich-structured LiCoO<sub>2</sub>-Super P-SACNT electrode could demonstrate outstanding cycle stability.

To obtain an accurate interpretation of the cell performance differences for the LiCoO<sub>2</sub>-Super P cathodes with and without SACNT conductive layers, the internal resistances of these two kinds of electrodes were investigated. The magnitude of the internal resistance (IR) can be characterized by the voltage drop, denoted as the IR-drop, when the charging process is switched to the discharging one. Fig. 6a and b shows the IR-drops of the LiCoO<sub>2</sub>-Super P-SACNT and LiCoO<sub>2</sub>-Super P cathodes charged and discharged at 0.1C in the 1<sup>st</sup> and 50<sup>th</sup> cycles. The voltage drops in the 1<sup>st</sup> cycle were almost imperceptible for both cathodes (0.013 V and 0.021 V). However, in the 50<sup>th</sup> cycle, there was an appreciable IR-drop of 0.042 V for the LiCoO<sub>2</sub>-Super P electrode (Fig. 6b). Generally speaking, the increase in the internal resistance after repeated cycling arises from the volume change and the generation of micro-gaps in the electrode. The conventional LiCoO<sub>2</sub>-Super P electrodes usually suffered from a local overcharge/overdischarge caused by the insufficient charge transportation, which would lead to a violent volume change and further compromise the integrity of the electrode. For the sandwich-structured LiCoO<sub>2</sub>-Super P-SACNT cathode, no obvious increment was observed in the IR-drop during

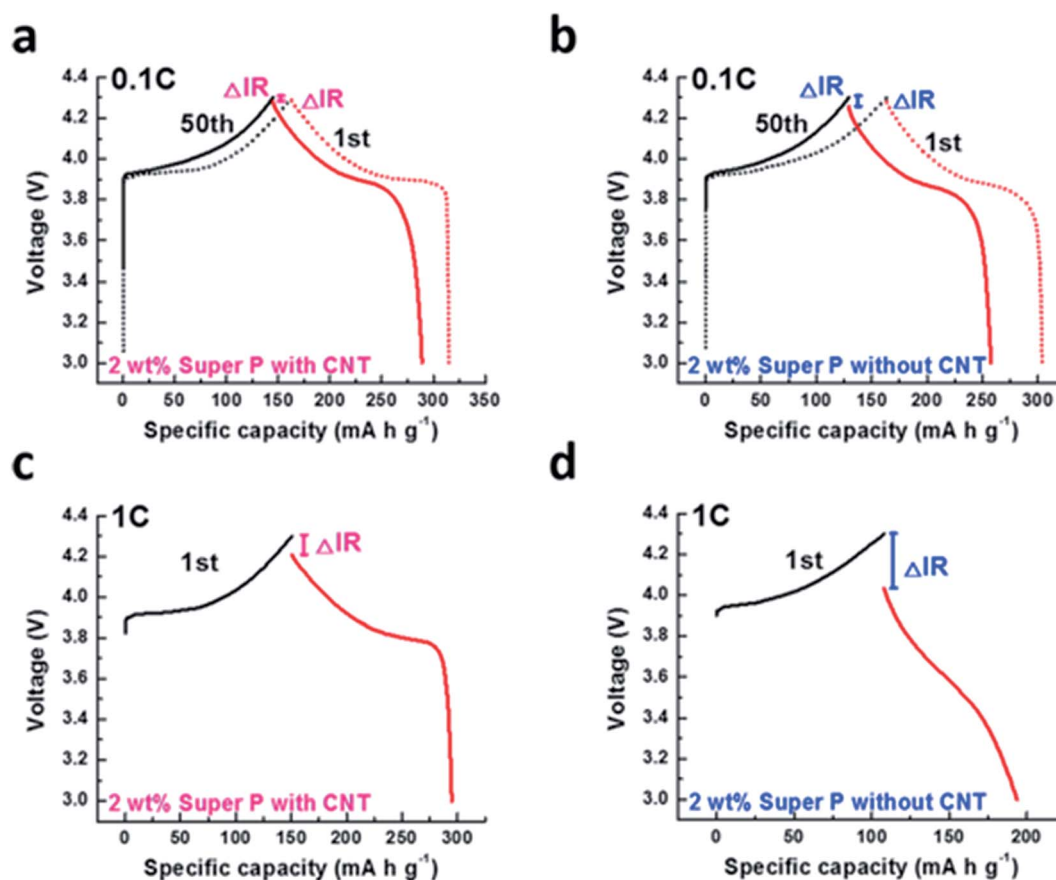


Fig. 6 IR drop data of the three-layer (a) LiCoO<sub>2</sub>-Super P and (b) LiCoO<sub>2</sub>-Super P-SACNT cathodes for the 1<sup>st</sup> and 50<sup>th</sup> cycles at 0.1C. (c) and (d) show the data of the same samples at 1C.

repeated charge and discharge. Actually, the change in the IR-drop even decreased a little to 0.019 V after 50 cycles, which may be ascribed to the improved wetting during the reactions. The results on the IR-drop during 0.1C cycles were consistent with the cycle performance of these two electrodes, giving further proof to the high efficiency of electron transfer in the LiCoO<sub>2</sub>-Super P-SACNT electrodes. Moreover, the contrast of the IR-drop became more distinct as the current rate was increased. Fig. 6c and d show the initial voltage profile at 1C for the LiCoO<sub>2</sub>-Super P-SACNT and LiCoO<sub>2</sub>-Super P cathodes. The LiCoO<sub>2</sub>-Super P cathode presented a more pronounced voltage drop (0.267 V) compared with the LiCoO<sub>2</sub>-Super P-SACNT cathode (0.094 V), reflecting the much larger terminal voltage and more severe polarization. Considering that both kinds of electrodes share almost the same amount of conductive additive as well as a similar thickness, the study on the IR-drop further confirms that the sandwich-structured electrodes with SACNT conductive layers is a more optimal electrode construction.

To further demonstrate the superiority of the SACNT conductive layers, a LiCoO<sub>2</sub>-10 wt% RCNT electrode was prepared as the control sample. The comparison of cycling (0.1C) and rate performance between the LiCoO<sub>2</sub>-10 wt% RCNT and the LiCoO<sub>2</sub>-2 wt% Super P-SACNT electrode is shown in Fig. S2a and b.† The LiCoO<sub>2</sub>-10 wt% RCNT cathode delivered a much smaller initial specific capacity of 136.1 mA h g<sup>-1</sup>, which was 20.6 mA h g<sup>-1</sup> lower than that of the LiCoO<sub>2</sub>-2 wt% Super P-SACNT electrode. The LiCoO<sub>2</sub>-2 wt% Super P-SACNT electrode demonstrated much better rate performance than the LiCoO<sub>2</sub>-10 wt% RCNT electrode. At 5C, the specific discharge capacity of the LiCoO<sub>2</sub>-2 wt% Super P-SACNT electrode was 123.6 mA h g<sup>-1</sup>, which was almost twice as that of the LiCoO<sub>2</sub>-10 wt% RCNT electrode. The marked difference in the cell performance of these two kinds of electrodes is ascribed to the distribution of CNTs. Fig. S2c† displays the SEM image of RCNTs, from which severe tube agglomeration was observed. This feature of the RCNT would lead to the non-uniform dispersion of conducting agents in the LiCoO<sub>2</sub>-10 wt% RCNT cathode, resulting in polarization and inferior cell performance. In comparison, in the sandwich-structured LiCoO<sub>2</sub>-2 wt% Super P-SACNT cathode, SACNTs are fully dispersed and form a homogeneous and efficient conductive network in the electrodes. The alternating stack of LiCoO<sub>2</sub> layers and SACNT films ensures the contact of active materials to the SACNT conductive layers, thus achieving sufficient electron transfer throughout

the electrodes and significant improvements on cycling and rate capability.

Table 1 summarizes the electrochemical performance of the sandwich-structured LiCoO<sub>2</sub>-Super P-SACNT electrode, and those of LiCoO<sub>2</sub> electrodes reported in the literature.<sup>45–49</sup> The sandwiched LiCoO<sub>2</sub>-Super P-SACNT electrode has many distinctive properties, including a simple fabrication process, a low content of the conductive additive (2 wt%), a high specific capacity with cycle stability (157.1 mA h g<sup>-1</sup> at 0.1C with capacity retention of 95% after 50 cycles), and high rate performance (109.6 mA h g<sup>-1</sup> at 10C). In particular, the sandwich-structured LiCoO<sub>2</sub>-Super P-SACNT electrodes delivered the best rate performances reported so far for commercial micro-sized LiCoO<sub>2</sub> particles.

The outstanding cell performance of the sandwich-structured LiCoO<sub>2</sub>-Super P-SACNT cathodes means a higher energy density in comparison with that of the LiCoO<sub>2</sub>-Super P cathodes containing the same amount of the conductive additive. Even though the specific capacity of conventional electrodes can be improved by adding more Super P, it is more difficult to achieve a corresponding increase in the energy density based on the whole electrode, including the conductive additive, binder and current collector, as extra inactive materials are also introduced. Fig. 7 compares the gravimetric energy densities of the LiCoO<sub>2</sub>-2 wt% Super P-SACNT electrode with those of the LiCoO<sub>2</sub>-5 wt% Super P electrode. The mass fraction of Super P (5 wt%) in the latter cathode was chosen as it exhibited a conductivity

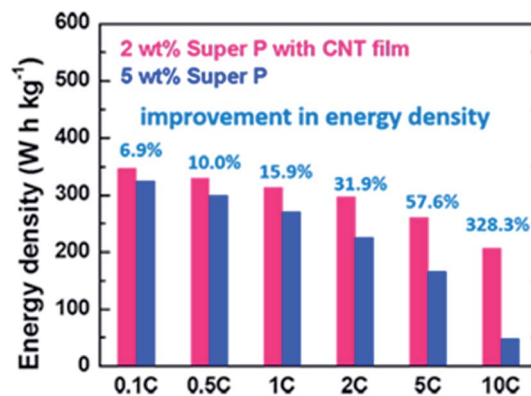


Fig. 7 Energy densities (based on the total mass of the electrode material layer and the current collector) of the LiCoO<sub>2</sub>-2 wt% Super P-SACNT and the sandwich-structured LiCoO<sub>2</sub>-5 wt% Super P electrodes (of the same thickness).

Table 1 Comparison of the electrochemical performances of the LiCoO<sub>2</sub> cathodes

| Cathode                                      | Capacity at low rate/mA h g <sup>-1</sup> | Capacity at high rate/mA h g <sup>-1</sup> | Capacity retention | Conducting additive | Reference |
|--|---|--|--------------------|---------------------|-----------|
| Sandwiched-LiCoO <sub>2</sub> -Super P-SACNT | 157.1 (0.1C)                              | 109.6 (10C)                                | 95% (50 cycles)    | 2 wt%               | This work |
| LiCoO <sub>2</sub> with carbon black         | 140.8 (0.1C)                              | <110 (0.5C)                                | <78% (50 cycles)   | 3 wt%               | 45        |
| LiCoO <sub>2</sub> nanowires                 | 148 (0.67C)                               | 113 (7C)                                   |                    | 10 wt%              | 46        |
| GN/SP LiCoO <sub>2</sub>                     | 146 (1C)                                  | 116.5 (5C)                                 | 96.4% (50 cycles)  | 1.2 wt%             | 47        |
| Flake-like LiCoO <sub>2</sub>                | 163 (0.1C)                                | <60 (5C)                                   | 93.9% (100 cycles) | 10 wt%              | 48        |
| 3D ordered macroporous LiCoO <sub>2</sub>    | 151.2 (1C)                                | ~90 (5C)                                   | 92% (50 cycles)    | 10 wt%              | 49        |

similar to that of the LiCoO<sub>2</sub>-2 wt% Super P-SACNT cathode. At each current rate, the sandwich-structured electrode exhibited the better result. In particular at 10C, the LiCoO<sub>2</sub>-2 wt% Super P-SACNT cathode delivered a gravimetric energy density as high as 206.7 W h kg<sup>-1</sup>, indicating an impressive improvement of 328.3%, compared with that of the LiCoO<sub>2</sub>-5 wt% Super P electrode (48.3 W h kg<sup>-1</sup>). Besides, the LiCoO<sub>2</sub>-2 wt% Super P-SACNT also showed an attractive volumetric energy density (based on the total volume of the cathode) of 695.8 W h L<sup>-1</sup>, which was more than a 310% increase than that of the LiCoO<sub>2</sub>-5 wt% Super P electrode. Moreover, unlike the conventional LiCoO<sub>2</sub>-Super P cathodes, the performance of the LiCoO<sub>2</sub>-wt% Super P-SACNT electrodes would not be undermined as the thickness was increased, because of the characteristics of the sandwich structure. As a result, an even higher energy density may be realized by repeating the procedure of coating the LiCoO<sub>2</sub> slurry and SACNT films alternatively more number of times. Considering the requirements for the commercial production of LIBs, such as a simple approach, low cost, and high energy densities, the use of SACNT films as conductive layers in large-scale production shows much promise.

## Conclusions

We have demonstrated a facile route to fabricate novel sandwich-structured electrodes with cross-stacked SACNT films as conductive layers. Based on the super-aligned characteristic, the SACNTs were sufficiently dispersed, forming a continuous and uniform conductive network. Thus, significant improvements on the conductivity as well as the cycle stability were observed when introducing only two layers of cross-stacked SACNT films into the single-layer LiCoO<sub>2</sub>-2 wt% Super P electrodes. Moreover, the well-designed sandwich-structured electrode ensured that each layer of LiCoO<sub>2</sub> particles could stick to the SACNT conductive layers. Unlike the conventional LiCoO<sub>2</sub>-Super P cathodes, sufficient electron transport was accessible to nearly all the active materials throughout the whole composite. Thus, polarization was effectively prohibited, and excellent cycle stability together with rate capability was realized in the sandwich-structured LiCoO<sub>2</sub>-Super P-SACNT electrodes. Moreover, the impressive performance was not affected by thickening the electrode. Thus, there was no need to sacrifice the thickness to obtain a decent specific capacity. Related to the improvement on charge transport, the decrease on the proportion of inactive materials, as well as the small limitation on the thickness, resulted in even higher energy densities with the sandwich-structured LiCoO<sub>2</sub>-Super P-SACNT cathodes. Considering the facile fabrication process and the outstanding performance, this novel strategy of sandwich-structured electrodes would have great potential on the practical production of LIBs.

## Acknowledgements

This work was supported by the National Basic Research Program of China (2012CB932301) and the NSFC (51472141).

## Notes and references

- 1 J. M. Tarascon and M. Armand, *Nature*, 2001, **414**, 359–367.
- 2 N. Nitta, F. X. Wu, J. T. Lee and G. Yushin, *Mater. Today*, 2015, **18**, 252–264.
- 3 J. L. Tebbe, T. F. Fuerst and C. B. Musgrave, *ACS Appl. Mater. Interfaces*, 2016, **8**, 26664–26674.
- 4 M. Armand and J. M. Tarascon, *Nature*, 2008, **451**, 652–657.
- 5 N. Imanishi, M. Fujiyoshi, Y. Takeda, O. Yamamoto and M. Tabuchi, *Solid State Ionics*, 1999, **118**, 121–128.
- 6 Y. Shimakawa, T. Numata and J. Tabuchi, *J. Solid State Chem.*, 1997, **131**, 138–143.
- 7 P. S. Herle, B. Ellis, N. Coombs and L. F. Nazar, *Nat. Mater.*, 2004, **3**, 147–152.
- 8 G. P. Wang, Q. T. Zhang, Z. L. Yu and M. Z. Qu, *Solid State Ionics*, 2008, **179**, 263–268.
- 9 S. Y. Chung, J. T. Bloking and Y. M. Chiang, *Nat. Mater.*, 2002, **1**, 123–128.
- 10 H. Tukamoto and A. R. West, *J. Electrochem. Soc.*, 1997, **144**, 3164–3168.
- 11 Z. H. Chen and J. R. Dahn, *J. Electrochem. Soc.*, 2002, **149**, A1184–A1189.
- 12 R. Dominko, M. Bele, M. Gaberscek, M. Remskar, D. Hanzel, S. Pejovnik and J. Jamnik, *J. Electrochem. Soc.*, 2005, **152**, A607–A610.
- 13 M. Okubo, E. Hosono, J. Kim, M. Enomoto, N. Kojima, T. Kudo, H. Zhou and I. Honma, *J. Am. Chem. Soc.*, 2007, **129**, 7444–7452.
- 14 J. K. Hong, J. H. Lee and S. M. Oh, *J. Power Sources*, 2002, **111**, 90–96.
- 15 F. Jiao, K. M. Shaju and P. G. Bruce, *Angew. Chem., Int. Ed.*, 2005, **44**, 6550–6553.
- 16 I. V. Thorat, V. Mathur, J. N. Harb and D. R. Wheeler, *J. Power Sources*, 2006, **162**, 673–678.
- 17 M. S. Bhuvanawari, N. N. Bramnik, D. Enslin, H. Ehrenberg and W. Jaegermann, *J. Power Sources*, 2008, **180**, 553–560.
- 18 X. L. Li, F. Y. Kang and W. C. Shen, *Carbon*, 2006, **44**, 1334–1336.
- 19 K. Sheem, Y. H. Lee and H. S. Lim, *J. Power Sources*, 2006, **158**, 1425–1430.
- 20 Q. A. Lin and J. N. Harb, *J. Electrochem. Soc.*, 2004, **151**, A1115–A1119.
- 21 J. Xu, G. Chen and X. Li, *Mater. Chem. Phys.*, 2009, **118**, 9–11.
- 22 K. Wang, Y. Wu, S. Luo, X. F. He, J. P. Wang, K. L. Jiang and S. S. Fan, *J. Power Sources*, 2013, **233**, 209–215.
- 23 X. B. Hu, M. H. Ma, R. G. Mendes, M. Q. Zeng, Q. Zhang, Y. H. Xue, T. Zhang, M. H. Rummeli and L. Fu, *J. Mater. Chem. A*, 2015, **3**, 23930–23935.
- 24 D. Zhao, Y. L. Feng, Y. G. Wang and Y. Y. Xia, *Electrochim. Acta*, 2013, **88**, 632–638.
- 25 A. K. Rai, J. Gim, S. W. Kang, V. Mathew, L. T. Anh, J. W. Kang, J. J. Song, B. J. Paul and J. Kim, *Mater. Chem. Phys.*, 2012, **136**, 1044–1051.
- 26 Q. T. Zhang, M. Z. Qu, H. Niu and Z. L. Yu, *New Carbon Mater.*, 2007, **22**, 361–364.

- 27 Z. Y. Chen, H. L. Zhu, W. Zhu, J. L. Zhang and Q. F. Li, *Trans. Nonferrous Met. Soc. China*, 2010, **20**, 614–618.
- 28 N. Naashima and T. Fujigaya, *Chem. Lett.*, 2007, **36**, 692–697.
- 29 X. M. Liu, Z. D. Huang, S. Oh, P. C. Ma, P. C. H. Chan, G. K. Vedam, K. Kang and J. K. Kim, *J. Power Sources*, 2010, **195**, 4290–4296.
- 30 S. Luo, K. Wang, J. P. Wang, K. L. Jiang, Q. Q. Li and S. S. Fan, *Adv. Mater.*, 2012, **24**, 2294–2298.
- 31 M. J. Ganter, R. A. DiLeo, C. M. Schauerman, R. E. Rogers, R. P. Raffaele and B. J. Landi, *Electrochim. Acta*, 2011, **56**, 7272–7277.
- 32 Y. L. Yin, C. H. Liu and S. S. Fan, *J. Phys. Chem. C*, 2012, **116**, 26185–26189.
- 33 K. L. Jiang, Q. Q. Li and S. S. Fan, *Nature*, 2002, **419**, 801.
- 34 K. L. Jiang, J. P. Wang, Q. Q. Li, L. A. Liu, C. H. Liu and S. S. Fan, *Adv. Mater.*, 2011, **23**, 1154–1161.
- 35 X. B. Zhang, K. L. Jiang, C. Teng, P. Liu, L. Zhang, J. Kong, T. H. Zhang, Q. Q. Li and S. Fan, *Adv. Mater.*, 2006, **18**, 1505–1510.
- 36 K. Liu, Y. H. Sun, P. Liu, J. P. Wang, Q. Q. Li, L. Liu, C. H. Liu, S. S. Fan and K. L. Jiang, *Nanotechnology*, 2009, **20**, 335705.
- 37 K. Liu, Y. H. Sun, L. Chen, C. Feng, X. F. Feng, K. L. Jiang, Y. G. Zhao and S. S. Fan, *Nano Lett.*, 2008, **8**, 700–705.
- 38 X. Y. Dai, A. J. Zhou, J. Xu, B. Yang, L. P. Wang and J. Z. Li, *J. Power Sources*, 2015, **298**, 114–122.
- 39 L. Li, H. J. Zhang, J. Yang, Y. P. Mu and Y. Wang, *Chem.–Eur. J.*, 2015, **21**, 19104–19111.
- 40 Q. Cao, H. P. Zhang, G. J. Wang, Q. Xia, Y. P. Wu and H. Q. Wu, *Electrochem. Commun.*, 2007, **9**, 1228–1232.
- 41 M. M. Shaijumon, E. Perre, B. Daffos, P. L. Taberna, J. M. Tarascon and P. Simon, *Adv. Mater.*, 2010, **22**, 4978–4981.
- 42 Q. Q. Li, L. Liu, C. H. Liu and S. S. Fan, *Adv. Mater.*, 2011, **23**, 1154–1161.
- 43 L. N. Zhang, C. Feng, Z. Chen, L. Liu, K. L. Jiang, Q. Q. Li and S. S. Fan, *Nano Lett.*, 2008, **8**, 2564–2569.
- 44 C. A. Frysz, X. P. Shui and D. D. L. Chung, *J. Power Sources*, 1996, **58**, 41–54.
- 45 J. H. Lee, S. B. Wee, M. S. Kwon, H. H. Kim, J. M. Choi, M. S. Song, H. B. Park, H. Kim and U. Paik, *J. Power Sources*, 2011, **196**, 6449–6455.
- 46 X. L. Xiao, L. M. Yang, H. Zhao, Z. B. Hu and Y. D. Li, *Nano Res.*, 2012, **5**, 27–32.
- 47 R. Tang, Q. B. Yun, W. Lv, Y. B. He, C. H. You, F. Y. Su, L. Ke, B. H. Li, F. Y. Kang and Q. H. Yang, *Carbon*, 2016, **103**, 356–362.
- 48 T. Wei, R. Zeng, Y. M. Sun, Y. H. Huang and K. V. Huang, *Chem. Commun.*, 2014, **50**, 1962–1964.
- 49 J. J. Peng, T. J. Zhang, H. M. Zhang, Z. Y. Zhang, Z. H. Li and G. T. Lei, *J. Solid State Electrochem.*, 2012, **16**, 3079–3085.